Tuning the scale factor and sensitivity of a passive cavity with optical pumping

Krishna Myneni*
RDMR-WSS, U.S. Army Research, Development, and Engineering Command, Redstone Arsenal, Alabama 35898, USA

David D. Smith
Spacecraft and Vehicle Systems Department, NASA Marshall Spaceflight Center, EV43, Huntsville, Alabama 35812, USA

Jamiu A. Odutola
Department of Natural and Physical Sciences (Chemistry), Alabama A&M University, Normal, Alabama 35762, USA

Charles A. Schambeau
Department of Physics, University of Alabama in Huntsville, Huntsville, Alabama 35899, USA
(Received 29 March 2011; revised manuscript received 25 April 2012; published 11 June 2012)

The pushing of the Fabry-Perot cavity modes by an intracavity medium of Rb vapor may be tuned with optical pumping. A second laser, propagating through the Rb vapor orthogonal to the intracavity beam, is used to modify the optical transmission of the Rb vapor. We demonstrate that the cavity scale factor may be switched from $S > 1$, on one side of its pole along the gain axis, to the other side of the pole, where mode splitting occurs, simply by changing the pumping transition. Continuous tuning of the cavity scale factor and sensitivity may be realized by varying the intensity and/or frequency of the pump beam.

DOI: 10.1103/PhysRevA.85.063813 PACS number(s): 42.60.Da, 42.50.Gy, 42.81.Pa, 33.80.Be

I. INTRODUCTION

In a recent paper [1], the phenomenon of mode pushing in a Fabry-Perot cavity by an intracavity medium with an absorption resonance was demonstrated. In the region of the absorption resonance, the peaks of the cavity modes are displaced from their empty cavity positions by an amount which depends on the anomalous dispersion associated with the medium's resonance. It was shown that the mode pushing is further enhanced by the variation in the absorption across the finite width of the cavity mode profile. When the modes are narrow compared to the atomic resonance, the mode positions are predicted by the standard mode pulling expressions [2–5] and there is no net enhancement in cavity sensitivity, defined here as the ratio of the scale factor enhancement to the normalized mode width. On the other hand, for mode widths comparable to the atomic linewidth, the modes can be reshaped, effectively pushing them even farther from the resonance and resulting in a net enhancement in sensitivity. These effects have particular relevance to optical ring cavity devices, in particular to optical gyroscopes and to ring laser gyroscopes. For these sensors the mode-pushing phenomenon may be used to enhance both the magnitude of the response to rotation (scale factor) and the signal-to-noise ratio [6–9]. Other potential applications include dispersion-enhanced optical interferometers for gravity wave detection, precision measurements of the Lense-Thirring frame-dragging effect [10], and enhanced strain sensing with an optical cavity [11].

Even though application of dispersive media to optical gyroscopes involves measuring the modified Sagnac effect in a rotating ring cavity, the essential physics of the mode pushing due to the intracavity dispersive medium can be studied simply with a one-dimensional cavity, for example, a Fabry-Perot cavity with tunable spacing. Neither is a high-finesse cavity required. In fact, a low-finesse cavity has the advantage that its mode widths are comparable to Doppler-broadened Rb transition linewidths, making observation of the dispersion enhancement considerably more straightforward, by maximizing the reshaping effect and increasing the bandwidth over which the dispersion enhancement occurs. Moreover, unlike the case of a laser where any anomalous dispersion that is introduced into the cavity by an absorbing medium is offset by increased normal dispersion in the gain medium, which necessitates the use of nonlinear and/or coherent mechanisms to observe the dispersion enhancement [9], in a passive cavity such a cancellation is precluded and the dispersion enhancement of the cavity can be readily observed with linear media.

For typical Gaussian or Lorentzian absorption resonances, the magnitude of the anomalous dispersion may be related to the on-resonance transmission, τ_0, and resonance width, γ. In conjunction with these medium parameters, the optical path length in the cavity, and loss factors of the cavity uniquely determine the cavity mode structure, with no dependence on intensity for a linear medium. Atomic vapor cells, used as the resonant intracavity medium, provide several desirable properties for investigating the enhancement of the scale factor and sensitivity, including a stable resonance frequency and a room-temperature Doppler-broadened resonance width compatible with the free spectral range (FSR) of tabletop optical cavities. Also, at low intensities relative to the saturation intensity of the relevant transition(s), the medium response is approximately linear. Previous studies using a Doppler-broadened resonance of hot alkali-metal vapor at high absorption (strong atom-cavity coupling) have demonstrated the phenomenon of mode splitting in a nonlinear regime [12]. In our earlier work using vapor cells containing isotopically pure ^{87}Rb at room temperature and of two different cell lengths

*krishna.myneni@us.army.mil

(3 and 8 cm), we demonstrated two types of cavity mode behavior near resonance in the approximately linear regime: fixed mode-pushing enhancement, and mode splitting.

The alkali-metal atomic vapor also enables modification of τ_0 by optical means. Optical hyperfine pumping between the two ground hyperfine levels may be used to increase or decrease the density of the atoms in the lower level seen by the cavity probe beam. Since the hyperfine pumping efficiency increases monotonically with the pump beam intensity, the pump intensity provides a useful control parameter for tuning the cavity scale factor. Furthermore, the time scale for changing τ_0 with optical pumping can be on the order of 1 μs or less, with moderate pump intensities. This allows for rapid tuning of the cavity optical response, which can be important for gyroscopic applications in high-dynamic-range environments. Although optical pumping modification of τ_0 is essentially a nonlinear phenomenon, when the pumping beam is orthogonal to the probe beam, the pumped intracavity vapor behaves as a linear medium with respect to the cavity transmission of the probe beam for weak probe intensity. In this paper, we demonstrate that optical pumping of the ^{87}Rb atom may be used to change τ_0 in a manner which is relatively independent of the resonance width and the empty cavity mode width and thereby achieve continuous tuning of the cavity scale factor and sensitivity. With this method, we demonstrate tuning the scale factor across its pole along the net gain axis, going from the region of enhanced but finite scale factor, $S > 1$, to the region of mode splitting, utilizing the same vapor cell. We discuss the behavior of S with the round-trip field gain in the cavity, g, and obtain an expression for the critical gain at which the pole occurs. We also discuss the limits of tuning g with optical hyperfine pumping and the time constant associated with this technique.

II. CAVITY SCALE FACTOR AND SENSITIVITY

Figure 1 shows the pushing of the cavity modes in the vicinity of a Gaussian optical resonance, for a Fabry-Perot cavity with an intracavity resonant medium. Physically, the shift in the cavity mode peak is due to a reshaping of the cavity mode near the resonance, both from the medium dispersion, $n(\Delta)$, and the variation of absorption, $\alpha(\Delta)$, across the width of the mode profile, with Δ being the detuning of the weak input laser from the resonant frequency of the medium,

$$\Delta \equiv \omega_L - \omega_0,$$

where ω_0 is the resonant frequency of the medium and ω_L is the laser frequency. The reshaping of the cavity mode may be treated, to first order, as a displacement of the peak and broadening of the feature. In addition to displacement of the peak and broadening of the mode profile, the phenomenon of mode splitting may also occur [Fig. 1(d)].

In order to discuss these effects quantitatively, we establish our notation and define some terms. Consider first an empty cavity, with mode peak frequencies, $\omega_{p,ec,}$, where p is the mode index. The frequencies may be given as offsets from the resonance frequency, ω_0,

$$\delta_p \equiv \omega_{p,ec} - \omega_0.$$

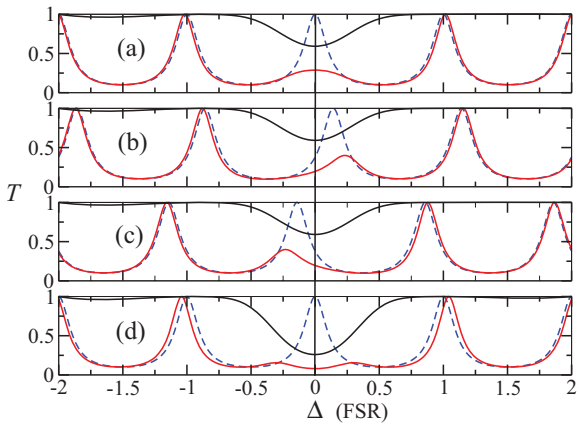

FIG. 1. (Color online) Cavity mode pushing and broadening by an intracavity resonant medium. The dashed curves show the empty cavity transmittance vs input laser detuning, Δ, for different detunings of an empty cavity mode from resonance. The solid curves at the top of each graph show the medium (single-pass) transmittance profile, and the solid curves at the bottom of each graph show the resulting cavity transmittance due to the presence of the resonant medium. In (a) an empty cavity mode peak coincides with the peak of an absorption resonance, $\delta_p = 0$, leading to a broadened and attenuated dispersive cavity mode. In (b) and (c) the empty cavity mode is detuned from the absorption peak by $\delta_p = \pm\gamma/4$, leading to dispersive cavity modes which are not only attenuated and broadened, but also have enhanced shifts in the peak positions. In (d) the mode detuning is $\delta_p = 0$ again, but the medium transmission, τ_0, has been further decreased, leading to mode splitting. The particular value of τ_0 at which mode splitting occurs depends on the resonance width and cavity parameters.

Similarly, the corresponding pushed modes in the same cavity containing a dispersive medium have offsets given by

$$\Delta_p \equiv \omega_p - \omega_0,$$

where ω_p is the angular frequency of the mode peak for the dispersive cavity. The medium is assumed to contain a single absorption resonance in the optical frequency region of interest.

Figure 2 shows the pushed mode detuning as a function of the empty cavity mode detuning, Δ_p vs δ_p, for a Fabry-Perot cavity with an intracavity dispersive medium. In a region of δ_p about the absorption resonance, Δ_p is dramatically enhanced. When the medium absorption is not strong enough to result in mode splitting, there is a one-to-one mapping between each empty cavity mode and a dispersive cavity mode. The cavity scale factor enhancement for a given mode p, may then be defined as

$$S_p \equiv S(\delta_p, g) \equiv \frac{d\Delta_p}{d\delta_p}. \quad (1)$$

For certain values of the round-trip field gain, $g(\Delta)$, the cavity scale factor enhancement at the resonance frequency can be increased dramatically and indeed become infinite. This is true even in the case of the passive cavity with a single beam, for which $g(\Delta)$ is always less than 1, as shown in Fig. 1. Furthermore, the width of the mode(s) nearest the resonance remains bounded by the combination of dispersion and absorption. Then it has been shown that the

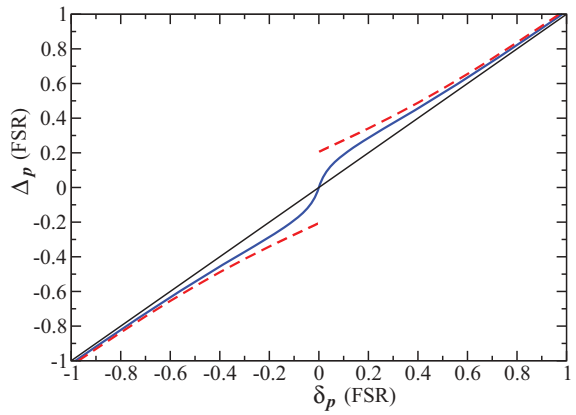

FIG. 2. (Color online) Pushed mode detuning, Δ_p, vs the empty cavity mode detuning, δ_p, for cavity mode p. The curves correspond to various choices of the round-trip field gain. The diagonal line represents the case of the empty cavity, $\Delta_p = \delta_p$. The solid curve shows the effect of a dispersive medium with an absorption resonance at $\delta_p = 0$. For this case, the dispersive cavity has a much larger shift in its mode position near the resonance than an empty cavity mode due to a change in length of the cavity. At $\delta_p = 0$, the cavity has a scale factor of $S(\delta_p = 0) = 3.4$. The dashed curve shows the effect of decreasing the round-trip gain below a critical value. If the on-resonance transmission of the medium, τ_0, is low enough, the cavity mode splits into two peaks.

cavity sensitivity may also be enhanced. We define sensitivity enhancement as

$$\zeta_p \equiv \frac{S_p}{W_p}, \tag{2}$$

where W_p is the mode width for dispersive cavity mode p, normalized to the empty cavity mode width. The sensitivity enhancement, ζ_p, is related to the signal-to-noise ratio in the measurement of mode offsets. Analytic expressions for S_p and W_p were given in [1] for the case of a Fabry-Perot cavity containing a dispersive medium and are reproduced here in the present notation,

$$S(\delta_p, g) = \frac{1}{\hat{n}_g(\Delta_p) + (1/t_c)[dF(\Delta_p, g)/d\Delta_p]}, \tag{3}$$

where $\hat{n}_g$ is the effective group index of the medium, t_c is the empty cavity round-trip time, and $F(\Delta_p, g)$ is an equivalent additional phase shift, given by

$$F(\Delta_p, g) = -\arcsin\left[\frac{1 - g(\Delta_p)^2}{2g(\Delta_p)} \frac{1}{t_c \hat{n}_g(\Delta_p)} \frac{d\ln[\tau(\Delta)]}{d\Delta}\bigg|_{\Delta=\Delta_p}\right]. \tag{4}$$

The physical origin of the additional phase shift, F, for a finite width cavity mode, is seen to be the *group velocity dispersion*, arising from the $d\ln(\tau)/d\Delta$ term in the above equation.

Both the scale factor enhancement, S_p, and the sensitivity enhancement, ζ_p, may be computed for a given mode detuning, δ_p, when the above expressions are combined with the transcendental expressions for the dispersive cavity mode peak detuning and mode width, derived from the dispersive cavity transmittance. The dispersive cavity mode peak detuning is given by

$$\Delta_p = \delta_p - (1/t_c)[\Phi(\Delta_p) + F(\Delta_p, g)], \tag{5}$$

where Φ is the additional round-trip phase shift in the cavity due to the dispersive medium. Under the assumption of linear dispersion, the above expression may easily be shown to be equivalent to the standard expression for mode pulling [2–5,7] in the limit where the reshaping factor F goes to zero, i.e., when the cavity mode width is much narrower than the atomic resonance linewidth, for example, in the case of a laser. The full width at half maximum for the pth mode in the dispersive cavity may be determined from the detunings of the half maxima of the transmittance function and are given by solution of

$$\Delta_{\pm,p} = \delta_p - (1/t_c)\{\Phi(\Delta_{\pm,p}) \mp 4\pi \arcsin[\sqrt{z(\Delta_p, \Delta_{p\pm1}) - y(\Delta_{\pm,p})}]\}, \tag{6}$$

with the definitions for $z(\Delta_p, \Delta_{p\pm1})$ and $y(\Delta_{\pm,p})$ given in [1].

Our earlier work made use of a resonant transition in ^{87}Rb vapor at room temperature. The optical resonance from this medium possessed a spectral width, γ, and peak field round-trip transmission value, τ_0, which were well-matched for demonstrating scale factor enhancement and cavity sensitivity enhancement for compact optical cavities with FSR of ~1 GHz or greater. The resonant transmission, τ_0, is a critical parameter in observing enhancement of the cavity scale factor and sensitivity, because it is related to the on-resonance net gain via $g_0 = ra\tau_0$, where r and a are frequency-independent cavity parameters, representing the round-trip mirror reflection and internal field attenuation, respectively. When $\tau_0 \approx 1$, there is little effect on the scale factor associated with the intracavity medium. When τ_0 is much less than unity, an empty-cavity mode coinciding with the resonance can be split into two modes [see Fig. 1(d)], displaced in opposite directions. The modes are also highly attenuated due to the strong absorption that accompanies the low transmittance. For intermediate values of τ_0, the cavity sensitivity is enhanced without mode splitting [13].

III. CRITICAL GAIN: SENSITIVITY AND SCALE FACTOR POLE

We consider only a *nonamplifying* cavity with an intracavity resonant medium. For such a cavity, the net round-trip field gain falls in the range, $0 < g_0 < 1$. Figure 3 shows the behavior of the on-resonance values of the cavity scale factor enhancement, $S_0 \equiv S_p(\delta_p = 0)$, the normalized mode width, $W_0 \equiv W_p(\delta_p = 0)$, and the cavity sensitivity enhancement, $\zeta_0 \equiv \zeta_p(\delta_p = 0)$, as a function of g_0. The mode width, W_0, is normalized to the empty cavity mode width and remains finite for all values of the gain. Two noteworthy values on the gain axis are the *critical gain*, $g_0 = g_c$, and the gain at which the medium becomes amplifying, $g_0 = ra$. The scale factor and sensitivity have poles at the critical gain, g_c. For values, $g_0 < g_c$, mode splitting occurs and the definition of S becomes ambiguous. For $g_0 > g_c$, S_0 falls until it reaches unity at $g_0 = ra$. At this point, the medium transmission is unity: $\tau_0 = 1$, and $S_0 = W_0 = \zeta_0 = 1$, which is equivalent to the empty cavity case. When the intracavity medium begins to

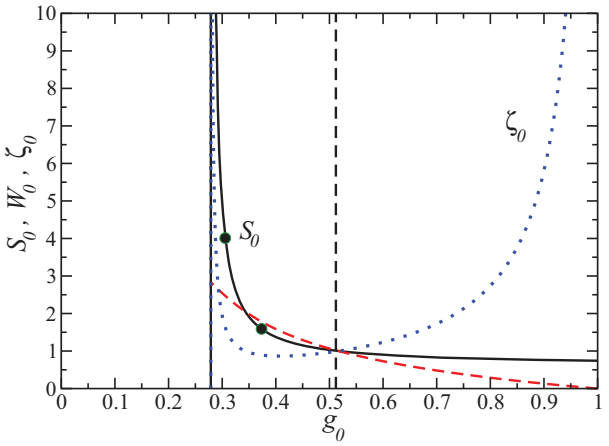

FIG. 3. (Color online) On-resonance behavior of scale factor enhancement, S_0 (solid), normalized mode width, W_0 (dashed), and sensitivity enhancement, ζ_0 (dotted), versus cavity round-trip field gain on resonance, g_0. For our choice of cavity parameters and absorption resonance width of $\Gamma_\alpha = 2\pi(0.564L/c)$, the critical gain occurs at $g_c = 0.278$ (solid vertical line). Note that $S_0 = W_0 = \zeta_0 = 1$, when $g_0 = ra$ (dashed vertical line). At this point, the medium becomes transparent, $\tau_0 = 1$, resulting in the empty cavity case. As the medium begins to amplify the intracavity field, the mode width, W_0, narrows, and the medium has normal dispersion, resulting in $S_0 < 1$. However, the sensitivity increases as the cavity lasing threshold is approached. Measurements of S_0 using a 3-cm ^{87}Rb vapor cell under different pumping conditions are indicated by the two points (solid circles) on the graph.

amplify, $g_0 > ra$, the scale factor enhancement continues to decrease below 1. However, the sensitivity enhancement, ζ_0, has another pole at the lasing threshold of the cavity, $g_0 = 1$, owing to the rapid narrowing of the mode width with increasing gain.

The common pole for S_0 and ζ_0 occurs at the critical gain value given by

$$g_c = \chi + \sqrt{1+\chi^2}, \tag{7}$$

where $\chi \equiv -(\hat{n}_g(0)t_c)^2\tau(0)/\tau''(0)$ is a parameter that depends only on absorption and dispersion and not on the cavity parameters r and a and τ'' is $d^2\tau/d\omega^2$. We may express χ directly in terms of the *material* absorption and dispersion, $\alpha(\Delta)$ and $n(\Delta)$, using the relations given in [1],

$$\chi = \frac{2}{\ell}\left(t_c + k_0\ell\,\frac{dn(\Delta)}{d\Delta}\right)^2\left(\frac{d^2\alpha(\Delta)}{d\Delta^2}\right)^{-1}\Bigg|_{\Delta=0}, \tag{8}$$

where ℓ is the round-trip path length in the medium, $\alpha(\Delta)$ and $n(\Delta)$ are related through the Kramers-Kronig dispersion relations, and Δ is the detuning of the intracavity field from the resonance frequency, ω_0. For a Gaussian absorption resonance, we may evaluate the expression for χ using the analytic expressions for $\alpha(\Delta)$ and $n(\Delta)$,

$$\alpha(\Delta) = \alpha_0 \exp\left[-4\ln(2)\Delta^2/\Gamma_\alpha^2\right], \tag{9}$$

where α_0 is the peak absorption coefficient and Γ_α is the full width at half maximum (FWHM) of $\alpha(\Delta)$. Note that Γ_α should not be confused with the FWHM of the transmittance profile, γ, although the two are related through the medium length. From the Kramers-Kronig relations [14], the corresponding analytic expression for the dispersion is

$$n(\Delta) = \mathrm{Re}\left\{1 + i\,\frac{c\alpha(\Delta)}{2(\Delta+\omega_0)}\mathrm{erf}\left(i2\sqrt{\ln(2)}\,\frac{\Delta}{\Gamma_\alpha}\right)\right\}. \tag{10}$$

Using the above, we obtain a convenient formula to compute χ in terms of the two resonance parameters, α_0 and Γ_α, and the two lengths, L and ℓ, the cavity round-trip length and the medium round-trip length, respectively,

$$\chi = \frac{\Gamma_\alpha^2}{4\ln\left(\frac{1}{2}\right)}\left(\frac{1}{\alpha_0\ell}\right)\left(\frac{L}{c} - \frac{2\alpha_0\ell}{\sqrt{\pi}\,\Gamma_\alpha}\sqrt{\ln(2)}\right)^2. \tag{11}$$

The critical gain is sensitively dependent on the width and depth of the absorption resonance. For fixed cavity parameters, L, r, and a, Eqs. (7) and (11) lead to a transcendental equation in the resonant round-trip transmission, τ_c, needed to achieve critical gain, g_c,

$$ra\tau_c = \frac{\Gamma_\alpha^2}{8\ln(2)\ln(\tau_c)}\left(\frac{L}{c} + \frac{4\ln(\tau_c)}{\sqrt{\pi}\,\Gamma_\alpha}\sqrt{\ln(2)}\right)^2. \tag{12}$$

For the cavity parameters used in this work, a FSR of $c/L = 981$ MHz, $r = 0.62$, and $a = 0.83$, and using $\Gamma_\alpha = 2\pi$ (555 MHz), corresponding to the absorption resonance width of the ^{87}Rb $F = 1 \rightarrow F'$ Doppler-broadened resonance near room temperature ($T \approx 24\,^\circ$C), equation (12) yields $\tau_c = 0.538$, or a critical gain of $g_c = 0.278$, consistent with the theoretical calculation of S_0 shown in Fig. 3. Note that this critical value of gain corresponds to an effective group index of $\hat{n}_g(0) = 0.672$, much greater than the value of $\hat{n}_g = 0$ predicted in [6] for the critical anomalous dispersion. The discrepancy arises due to the effect of the variation of absorption with Δ, across the finite width of the cavity mode, which was not considered in the earlier work.

Figure 3 also shows the operating points of measurements performed in the 3-cm Rb vapor cell. With the longer 8-cm cell, the low transmission, $\tau_0 = 0.29$, on resonance with the Doppler-broadened $F = 2 \rightarrow F'$ transitions placed us to the left of the scale factor pole, $g_0 < g_c$, well into the mode-splitting regime. On the other hand, when a shorter 3-cm cell was used, τ_0 became high enough to place us near the pole on the opposite side, $g_0 > g_c$, giving both an enhanced scale factor, $S_0 = 2.4$, and an enhanced sensitivity, $\zeta_0 = 1.4$, for the chosen experimental parameters.

We note also that, for a given g_0, the range of δ_p over which the scale factor enhancement occurs, i.e., the bandwidth of scale factor enhancement, depends not only on the width of the resonance profile, γ, but also on the value of S_0. Figure 4 shows the dependence of S_p vs δ_p, with a width denoted by w_s. As S_0 is increased, by decreasing τ_0, the width w_s decreases. Although we have not obtained an analytic expression for the width w_s, numerical calculation of the scale factor-bandwidth product, $S_0 w_s$, shows that it is approximately constant in the region $g_c < g_0 < ra$, except near the end points.

IV. TUNING VIA OPTICAL PUMPING

Our earlier analysis modeled the atomic vapor as an inhomogeneously broadened collection of identical two-level atoms and ignored saturation and pumping effects, even though

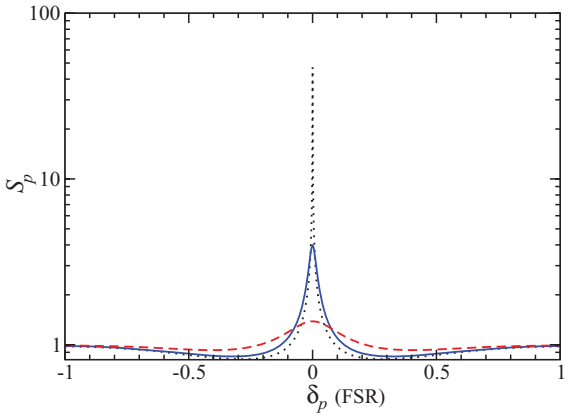

FIG. 4. (Color online) Scale-factor dependence on empty cavity mode detuning, $S(\delta_p,g)$ vs δ_p, for several gain values, $g(0)$, and our cavity parameters and resonance width (see Fig. 3). The scale factor enhancement is unity at large mode detunings, shown in units of cavity FSR, and has a maximum, S_0, when the empty cavity mode exactly coincides with the absorption resonance of the medium. The three curves show $S(\delta_p,g)$ for (a) $g_0 = 0.279$, $S_0 = 47$ (dotted line); (b) $g_0 = 0.306$, $S_0 = 4.0$ (solid line); and (c) $g_0 = 0.398$, $S_0 = 1.4$ (dashed line).

the D_2 transition in ^{87}Rb at room temperature involves multiple transitions between the multiple hyperfine and Zeeman levels. Homogeneous broadening via power-broadening was also ignored since the intracavity intensity was measured to be below the saturation intensity [15]. Even in the absence of significant saturation effects by the intracavity beam, pump-probe effects due to optical pumping may modify the effective absorption and index of refraction presented by the medium. The richness of optical pumping effects involving the transfer of an atom between its ground hyperfine levels and Zeeman sublevels, via an optical transition to an excited state, affords us a great deal of flexibility in tailoring the response of the medium to the intracavity field and, therefore, tuning the cavity response. Optical pumping by a second laser may be used to either increase or decrease the effective atom density seen by the probe (intracavity) beam. Figure 5 shows the four different combinations of pump and probe transitions used in our experiments. Optical pumping between the $F = 1$ and $F = 2$ ground levels can occur via excitation to and decay from the upper $F' = 1$ and $F' = 2$ hyperfine levels.

An upper limit on the tuning range of τ_0 and, consequently, g_0, afforded by the optical pumping method can be estimated by making the simplification that the atoms have a Maxwellian distribution of longitudinal velocities, v_l, i.e., velocity with respect to the intracavity beam, but have zero transverse velocity, v_t (zero velocity with respect to the pump beam). Then the incoherent rate equations describing the laser-atom interaction with the multilevel atom may be applied to a single velocity group, $v_t = 0$, over the practical range of intensity. The change in atom density in a given lower hyperfine level, and the accompanying change in absorption coefficient seen by the cavity probe beam, due to the presence of the pump beam, may be obtained as a function of time. Since the pumping of an atom which transits through the pump and probe regions depends on the interaction time of the atom with the pump

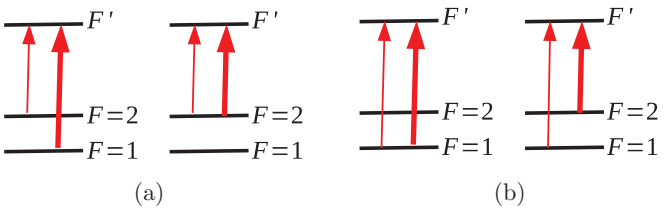

FIG. 5. (Color online) Optical pumping schemes for the ^{87}Rb D_2 transition. (a) For the intracavity field tuned to $F = 2 \rightarrow F'$ (thin arrow), the pump beam (thick arrow) may be tuned to the $F = 1 \rightarrow F'$ to increase the population of the lower $F = 2$ hyperfine level, decreasing τ_0 for the intracavity field, or the pump beam may be tuned to $F = 2 \rightarrow F'$, to decrease the population of the lower $F = 2$ level, increasing τ_0 for the intracavity field. (b) Similarly for the intracavity field tuned to $F = 1 \rightarrow F'$, the pumping transition may be selected to either decrease τ_0 or to increase τ_0. A linearly polarized pumping beam is used, and the degree of pumping is controlled by adjusting the intensity of the pump beam. Multiple hyperfine levels and Zeeman sublevels participate in the pumping process.

beam, it is not the steady-state solutions to the rate equations which are of interest. Rather, the populations most relevant to the experiment are the solutions of the rate equations at the particular time which represents the average interaction time of the atom in the pump beam. Figure 6 shows the time-dependent populations for one of the cases described in Fig. 5 at a given pump intensity. The change in atom density, for the given lower level of the intracavity field, can then be estimated as a function of time. The fractional change in the resonant absorption coefficient is given by

$$\frac{\Delta\alpha_0}{\alpha_0} = \frac{n_F - n_{F,0}}{n_{F,0}}, \tag{13}$$

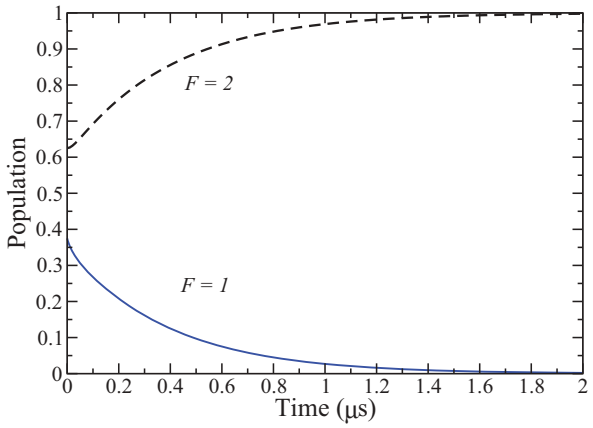

FIG. 6. (Color online) Time-dependent populations for optical pumping. The populations of the lower $F = 1$ and $F = 2$ levels are shown in the presence of a pumping beam tuned to the $F = 1 \rightarrow F' = 2$ transition in ^{87}Rb. The initial populations are thermal equilibrium values at room temperature. An eight-level model, including Zeeman sublevels, was used to compute the dynamics. Shown in the graph are the sum of the $F = 1$, m_F sublevel populations (solid line) and the population of the $F = 2$ level (dashed line). Nearly complete pumping is achieved for an atom with transverse velocity, $v_t = 0$, within a pumping time of 2 μs.

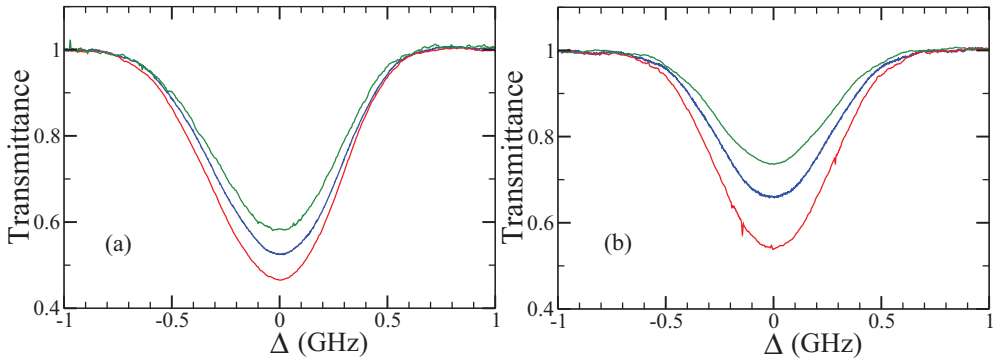

FIG. 7. (Color online) Single-pass transmittance versus laser detuning from resonance (Δ). (a) The middle curve is the transmittance of the vapor cell with no repumping beam, with a single-pass transmittance of 0.52, corresponding to a round-trip $\tau_0 = 0.52$, while the transmittance below and above correspond to the two cases shown in Fig. 5(a), with the pumping beam ($\langle I \rangle \sim 2\text{mW/cm}^2$) on the $F = 1 \rightarrow F'$ transition ($\tau_0 = 0.47$) and $F = 2 \rightarrow F'$ transition ($\tau_0 = 0.58$), respectively. The resonance widths also change with the repumping beam parameters, by about 2%. Given $ra = 0.458$ for our experiment, we can tune the cavity round-trip field gain over the range $0.22 < g_0 < 0.26$. (b) For the case of the intracavity laser field tuned to the $F = 1 \rightarrow F'$ transition, with the pumping beam on the two different transitions shown in 5(b), we obtain a tuning range $0.25 < g_0 < 0.34$.

where n_F is the time-dependent population of the lower hyperfine level, F, for the intracavity probe beam, and $n_{F,0}$ is the initial population at the beginning of optical pumping. Nearly complete pumping occurs on a time scale of 2 μs for the parameters used in the calculation of Fig. 6. This is the same order of magnitude as the transit time of an atom in the pump beam, for a thermal vapor and pump beam diameters of a few mm. Thus, even at pump beam intensities on the order of the typical saturation intensity for closed transitions, the atom will be fully pumped. For any (lower) pump intensity, complete optical pumping will occur for a long-enough atom-pump interaction time. Therefore, to evaluate the tuning limits, we may assume the atom becomes fully pumped and take $n_F = n_0$, where n_0 is the total atom density. Assuming thermal equilibrium, $n_{F,0}$ is given by

$$n_{F,0} = \frac{2F+1}{\sum_f (2f+1)}, \tag{14}$$

where $f = 1,2$ for ^{87}Rb. For complete pumping, n_F will be either 0 or n_0, depending on the selected pumping transition. Then the quantity $\Delta\alpha_0/\alpha_0$ has a theoretical maximum tuning range from $-1 \rightarrow 5/3$ when the intracavity field (probe) is tuned to the $F = 1 \rightarrow F'$ transitions and a maximum tuning range from $-1 \rightarrow 3/5$ when the probe is tuned to the $F = 2 \rightarrow F'$ transitions. A measurement of α_0 for the probe beam can then be used to determine the theoretical maximum tuning range of τ_0, via optical pumping in ^{87}Rb. For example, single-pass transmittance measurements made at low probe power in a 3-cm vapor cell, given in Fig. 7, yield $\alpha_0 = 13.9\ \text{m}^{-1}$ for the $F = 1 \rightarrow F'$ probe, and $\alpha_0 = 21.5\ \text{m}^{-1}$ for the $F = 2 \rightarrow F'$ probe. Thus, τ_0 has a theoretical maximum tuning range for this cell and probe beam of $0.33 \rightarrow 1$ for the $F = 1 \rightarrow F'$ probe and a slightly reduced maximum tuning range of $0.36 \rightarrow 1$ for the $F = 2 \rightarrow F'$ probe.

Quantitative estimates of the tuning range in τ_0 in a true thermal vapor are more difficult to compute. The problem does not have to do with simply having to compute the pumping effects over the entire range of transverse velocities. For a narrow linewidth pump laser, velocity-selective optical pumping predicts the transfer between ground-state hyperfine levels of only narrow velocity groups, v_t, as shown in Fig. 8. Since v_t is independent of v_l, these velocity groups constitute only a small fraction of the atoms seen by the intracavity field. Hence, one might expect that transverse optical pumping would not lead to sizable changes in τ_0. Frequency modulation of a laser as a means of achieving high efficiency pumping in a thermal vapor of alkali-metal atoms has been studied [16].

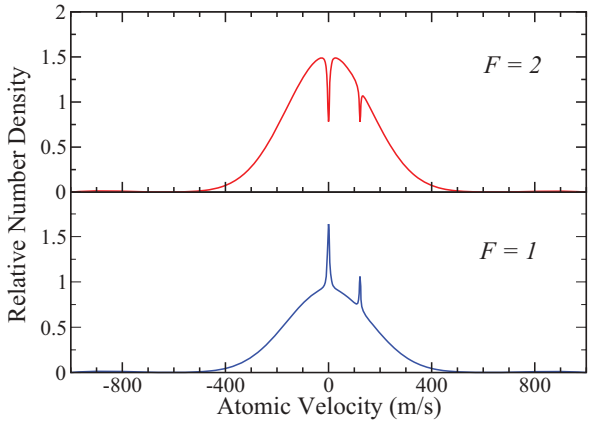

FIG. 8. (Color online) Velocity-selective optical pumping with a π-polarized pump beam locked to the $F = 2 \rightarrow F' = 2$ transition. The calculated relative number density of ground-state ^{87}Rb atoms is shown as a function of the atom velocity, with respect to the pump, for the two ground hyperfine levels. Two narrow velocity groups from the lower $F = 2$ level are transferred to the lower $F = 1$ level. A pump beam intensity of 2.0 mW/cm^2 and an atom-pump interaction time of 1.5 μs were used in the calculation. The incoherent rate equations for the level populations were solved numerically, using all relevant Zeeman sublevels in the $F = 1$, $F = 2$, and $F' = 2$ hyperfine levels. With the pump beam locked to the $F = 1 \rightarrow F' = 2$ transition, the dips in the above figure become spikes, and vice versa, although not with the same magnitudes.

In practice, significant changes in the effective atom density seen by the intracavity field occur even when using a narrow linewidth pump laser in the transverse configuration. Two effects, which are dependent on the details of the pump beam and vapor-cell geometry, conspire to diminish the effects of the velocity-selective optical pumping: (1) ineffective relaxation of the atom's internal state after a wall collision and (2) velocity-changing collisions due to atom-wall collisions and, to a lesser extent in low-pressure vapor cells, atom-atom collisions during the measurement time. If the collision of a pumped atom with the vapor-cell wall is not effective at rethermalizing the internal state of the atom, the assumption that the atom enters the pump beam in a thermal equilibrium state, that is, with all hyperfine sublevels populated according to the Boltzmann distribution, is invalid for the rate equation calculations. Furthermore, if a velocity-changing collision occurs for the pumped atom so that the velocity, v_l, is scattered to a new longitudinal velocity, v_l', then the effective density of pumped atoms, seen by the intracavity field, increases. Such effects have been noted previously [17] and are consistent with our observations of the change in τ_0 using a transverse pump beam. Fortunately, these effects are beneficial, rather than detrimental, for tuning the cavity response via optical pumping.

Figure 6 shows the time-dependent populations of the two lower hyperfine levels in the transition diagrams of Fig. 5. The populations were computed for a pump beam on the $F = 1 \rightarrow F' = 2$ transition and a probe beam on the $F = 2 \rightarrow F' = 3$ transition. In general, for π-polarized pump and probe beams inducing these transitions, a 16-level model is needed to account for the effects of Zeeman pumping. However, our calculations showed that inclusion of Zeeman pumping effects did not significantly alter the time scale for transfer of population from the $F = 1$ to the $F = 2$ lower hyperfine levels. We used, instead, an 8-level model to include the Zeeman sublevels of the lower $F = 1$ level, a single effective lower $F = 2$ level, the three relevant Zeeman sublevels of the upper $F' = 2$ level, and a single effective upper $F' = 3$ hyperfine levels. In Fig. 6, the intracavity probe beam intensity was taken to be zero to investigate the low intensity probe limit. Hence, the dynamics induced by the probe beam are not relevant for this figure, and the $F = 2$ and $F' = 3$ level populations need not be tracked. The intensity of the pump beam was taken to be 2 mW/cm^2. For the temperature of our experiment and our relevant beam width for the repumping beam, the average drift time for an atom in the repumping beam, prior to entering the cavity probe beam, was approximately 1.5 μs. Hence, nearly maximum optical pumping efficiency is achieved for a single velocity group.

V. EXPERIMENT

The single-pass transmittance spectra of the vapor cell, outside of the cavity, are shown in Fig. 7 for the two sets of Doppler broadened hyperfine transitions, $F = 1 \rightarrow F'$ and $F = 2 \rightarrow F'$. For each case, repumping may be used to either increase or decrease the population of the level, depending on which lower level is resonant for the pump beam transition. Figure 7 shows that the on-resonance transmittance, τ_0, may be increased or decreased by the presence of the repumping beam, about the value of τ_0 in the absence of the pump beam. These single-pass transmittance measurements of the resonance, made without the optical cavity, give a good idea of the tunability of τ_0, but may not coincide exactly with the actual conditions of the experiments performed with the cavity, owing to reproducibility of the vapor-cell temperature, and the difference in intracavity beam intensity compared to the single-pass intensity, discussed below. It should be noted that the repumping beam does not significantly alter the resonance width. Hence, the anomalous dispersion will also change inversely with the change in transmittance.

The mode-pushing experiment is shown in Fig. 9 and the basic method of obtaining the cavity mode spectra is the same as in our earlier work. However, a second narrow linewidth laser (linewidth of ~1 MHz) provides a pump beam of adjustable intensity and locked-in frequency to one of the four cases shown in Fig. 5. The pump beam is first expanded and then focused via a 15-mm-focal-length cylindrical lens into a line inside the intracavity vapor cell (see Fig. 9). Note that the propagation direction of the pump beam is orthogonal to that of the probe beam, and the focused line is parallel with the probe beam. The focused line extends across a $1/e$ width of 6 mm in the transverse direction, along the length of the cell, and a $1/e$ width of 0.25 mm in the vertical direction, along the direction of focus. With a typical power

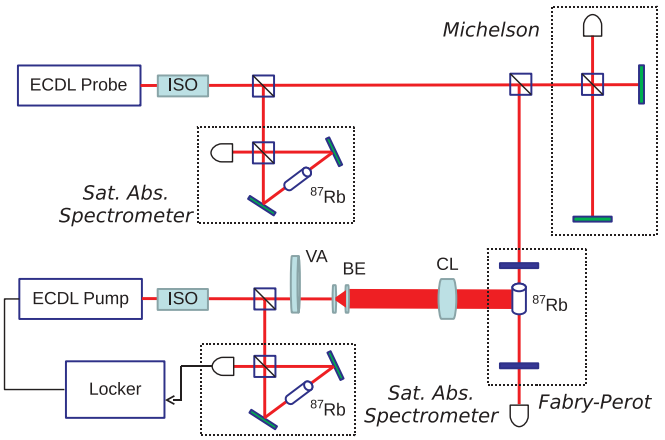

FIG. 9. (Color online) The experimental configuration shown above includes a tunable diode laser which acts as the intracavity probe laser and a frequency-locked pump laser to produce optical hyperfine pumping of atoms in the intracavity ^{87}Rb vapor cell. Separate saturated-absorption spectrometers provide a frequency scale for the swept probe laser and a frequency reference for locking the pump laser. A Michelson interferometer, with unequal arm lengths, provides a fringe pattern useful for frequency scale linearization, as the probe laser is swept in frequency. The cavity mode profile is observed by recording the Fabry-Perot transmittance as the probe laser is swept. The peak transmission of the intracavity cell is adjusted above or below that of the unpumped vapor cell by selection of the saturated-absorption resonance to which the pump laser is locked and tuned continuously via the variable attenuator (VA). Additional elements in the setup include optical isolators (ISO), a beam expander (BE), and a cylindrical lens (CL).

in the pump beam of 12 mW, the average pump intensity near the probe beam is determined to be 38 mW/cm^2. The average pump-beam intensity across the entire cell is roughly 2 mW/cm^2. The average pump intensity is significant, since our optical pumping calculations show that, even at such low pump intensities, the atom can be nearly completely pumped for short interaction times of a few microseconds. Thus, the pumping for resonant atoms during their transit time into the probe field, is nearly complete. The orthogonality of the pump beam with the probe beam means that all velocity groups sampled by the probe beam are pumped; that is, while velocity-selective pumping occurs along the pump propagation axis (z), the pumping is not velocity-selective along the probe propagation axis (x). As a consequence of this arrangement, no additional resonances occur in the probe spectrum. In contrast, using a collinear pump and probe configuration gives rise to additional velocity-selective pumping resonances in the probe spectrum [18,19]. For the measurements presented here, we used only the 3-cm, isotopically pure ^{87}Rb vapor cell.

The pump and probe beams were overlapped; however, it was not necessary that the focused line of the pump beam intersect perfectly with the probe beam. By varying the position of the cylindrical lens along the z axis, we could control the displacement of the focused pump beam within the cross section of the probe profile. The optimum position of the focused pump, to obtain the maximum change in the cavity mode peak, was determined by repetitively sweeping the probe laser frequency through the cavity mode nearest resonance and observing the mode height while positioning the pump focusing lens.

Determination of the plane parallel Fabry-Perot cavity parameters, r and a, was discussed in our previous work [1]. Due to degradation of the mirror coatings used previously, new substrates were coated with thin gold films of about 60 nm. The present values of r and a were found to be 0.62 and 0.83, respectively. For the results reported in this work, the empty cavity round-trip length, L, was 0.31 m, and the finesse of the cavity, with the intracavity vapor cell included, was measured to be about 5.5 at a detuning of several GHz off resonance. The probe beam intensity, as in our earlier experiment, was kept low to avoid strong saturation effects on the absorption line shape. For the probe tuned to the $F = 2 \rightarrow F'$ transition, the incident optical intensity onto the cavity was approximately 60 mW/cm^2. Despite the large input intensity with respect to the saturation intensity ($I_{\rm sat} = 3.0$ mW/cm^2) for ^{87}Rb on the $F = 2 \rightarrow F' = 3$ transition, the intracavity intensity, as inferred from the transmitted intensity off the cavity mode peak on resonance, was ~0.03 mW/cm^2, more than an order of magnitude below $I_{\rm sat}$, typically. The low intracavity laser intensity, relative to the incident intensity, is attributed to the effective values of r and a for our cavity. The effect of the nonlinear intensity-dependent absorption of the medium on the scale factor enhancement, S_0, has not been studied in detail, and we plan to provide experimental and theoretical results on this effect elsewhere.

VI. RESULTS

Cavity mode shifts using a 3-cm, isotopically pure ^{87}Rb vapor cell were measured with and without the optical pumping beam [20]. Data were obtained with all four pumping cases shown in Fig. 5. For the intracavity probe beam swept through each of the two Doppler-broadened transmission resonances, the repumping beam is locked to one of two different hyperfine transitions: one which results in increased ground-state population seen by the probe (decreased τ_0) and one which results in decreased ground-state population seen by the probe (increased τ_0). Measured dispersive cavity mode-shift curves, $\Delta_p(\delta_p)$, are shown in Figs. 10 and 11. The empty cavity detunings δ_p were determined from modes that were off resonance by a few FSRs near the end of the frequency scan. Consequently, the error in the δ_p values was dominated by frequency scale nonlinearity. On the other hand, measurements of dispersive cavity detunings Δ_p were limited to the region near resonance where the frequency scale was approximately linear. The error in the Δ_p values was, therefore, dominated by the resolution of mode peak positions. The measured mode shifts vs empty cavity mode detunings were fit by the theoretical model for Δ_p, given in [1], using two

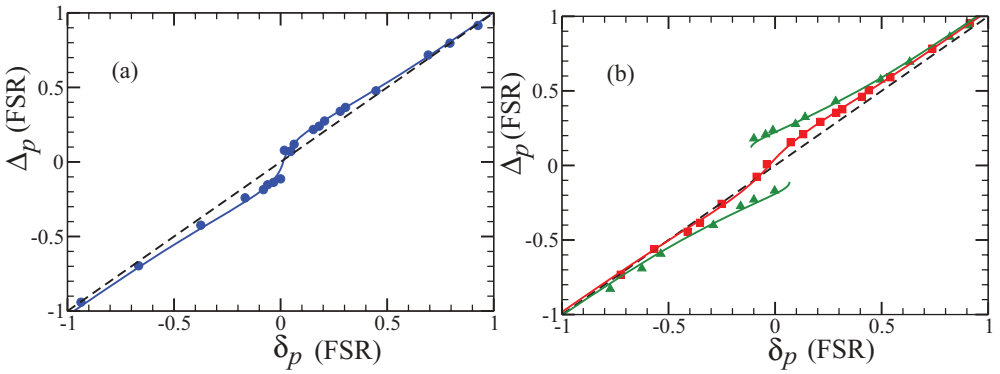

FIG. 10. (Color online) Mode-shift measurements for the $F = 1 \rightarrow F'$ intracavity probe field: (a) data (circles) and fit (solid line) for a 3-cm cell with no pump beam present ($S_0 = 4.0$), (b) data (squares) and fit for 3-cm cell with pump beam locked to the $F = 1 \rightarrow F' = 2$ transition ($S_0 = 1.59$), and data (triangles) and fit with the pump beam locked to the $F = 2 \rightarrow F' = 2$ transition (mode-splitting region). The dashed line, shown for reference, is the empty cavity response.

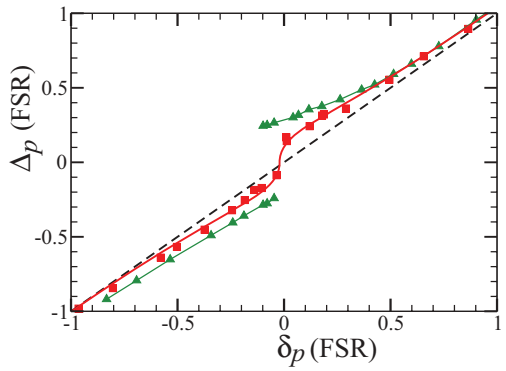

FIG. 11. (Color online) Mode-shift measurements for the $F = 2 \rightarrow F'$ intracavity field. Data (squares) and fit (solid line) for the pump beam locked to the $F = 2 \rightarrow F' = 2$ transition reveal that decreased absorption by the medium pushes the operating point away from the critical gain sufficiently to give a finite but enhanced scale factor, $S_0 = 14.8$. With the pump locked to the $F = 1 \rightarrow F' = 2$, the absorption has increased sufficiently to observe clear mode splitting in the data (triangles).

fitting parameters: the peak absorbance, $\alpha_0 \ell$, and an offset for the δ_p values, δ_{ofs}, to account for a possible systematic error in the determination of the empty cavity mode detunings. The cavity parameters, r, a, and t_c were fixed to experimentally determined values, given previously. Also, the resonance width, Γ, was fixed to the experimentally determined width for the corresponding resonance (see Fig. 7). From the fitted Δ_p vs δ_p curve, we obtained the best fit estimates of τ_0, S_0, and the normalized mode width at zero detuning, W_0. Estimated uncertainties in the fitted parameters, and parameters derived from these values, were determined from the uncertainties in the Δ_p [upper limit of $\pm 2\pi(4$ MHz)] and δ_p [$\pm 2\pi(5$ MHz)] values.

Measurements for the unpumped vapor cell are shown in Fig. 10(a). For these data, the cavity modes are detuned about the D_2, $F = 1 \rightarrow F'$ Doppler-broadened resonance. The fitted values are $\tau_0 = 0.592 \pm 0.007$, $S_0 = 4.01 \pm 0.53$, and $W_0 = 2.47 \pm 0.05$. The pair of values (τ_0, S_0) from this data set is shown in Fig. 3, overlaying the predicted behavior of S_0 vs τ_0. The sensitivity enhancement factor for this data is greater than unity, $\zeta_0 = S_0/W_0 = 1.62$. With optical pumping of the vapor cell, the cavity mode shifts are substantially modified, as shown in Fig. 10(b). Two pumping cases are shown on the graph. With the pump locked to the $F = 1 \rightarrow F' = 2$ transition, atoms in the vapor cell are transferred from the ground-state $F = 1$ hyperfine level to the ground-state $F = 2$ level. The pumping decreases the density of atoms seen by the intracavity field, which interacts with the $F = 1$ atoms, increasing the value of τ_0. For this case, we obtained $\tau_0 = 0.723 \pm 0.009$, a reduced scale factor enhancement of $S_0 = 1.59 \pm 0.05$ and $W_0 = 1.78 \pm 0.04$. The sensitivity enhancement factor is now below unity, $\zeta_0 = 0.89$. With the pump locked to the $F = 2 \rightarrow F' = 2$ transition, the density of atoms in the $F = 1$ lower level is increased, and τ_0 is found to be decreased to a value of 0.41, well below the critical value seen in Fig. 3. For this case, the cavity mode is split into two peaks, and S_0, W_0, and ζ_0 are no longer meaningful.

Data were also obtained with cavity modes detuned from the D_2, $F = 2 \rightarrow F'$ Doppler-broadened resonance, as shown in Fig. 11. For this resonance, the unpumped vapor cell had a large-enough absorption for the mode to be just slightly above the splitting point. It should be noted that in our previously reported results for an unpumped 3-cm vapor cell [1], the absorption of the same unpumped cell was somewhat lower, leading to a finite and small-scale factor ($S_0 = 2.4$) for this case. The difference in operating point between the earlier measurements and the present ones is attributed to a difference in the ambient temperature, leading to a sufficiently large change in the absorption profile for the cell. Ambient temperature variations occur on a slow time scale of hours in our laboratory, and they are not expected to lead to variations in absorption during the measurements on the effects of pumping presented here. Nevertheless, temperature dependence of the cell absorption can lead to large variations in the scale factor. A typical operating temperature for our measurements is $T = 24.4\,^{\circ}$C, with variations from day to day of a couple of degrees Celsius.

Only data with the pump field present, corresponding to the two cases in Fig. 5(a), are shown in Fig. 11. With the pump beam locked to the $F = 2 \rightarrow F' = 2$, the fitted parameters were $\tau_0 = 0.529 \pm 0.009$, $W_0 = 2.84 \pm 0.07$, and $S_0 = 14.84$ (with errors of $+30.21$ and -5.82), corresponding to a sensitivity enhancement factor of $\zeta_0 = 5.23$. The sparsity of data in the region of enhancement leads to the large uncertainty in the fitted value of S_0. Note that the pair of values (τ_0, S_0) from this fit are not shown in Fig. 3 since the calculated curves in that figure are specific to the width of the $F = 1 \rightarrow F'$ resonance. With the pump beam locked to the $F = 1 \rightarrow F' = 2$ resonance, the increased population of the lower $F = 2$ level gives an increased absorption ($\tau_0 = 0.33$), resulting in clearly observable mode splitting.

VII. CONCLUSIONS

We have demonstrated tuning of the cavity response for a cavity containing a thermal atomic vapor through the use of optical pumping of the intracavity medium. By selecting the pumping transition (pump frequency) and pump beam intensity and size, we have shown that it is possible to change the optical transmission of the intracavity ^{87}Rb vapor, τ_0, by a sufficient amount to tune the cavity round-trip field gain from below the critical gain, $g_0 < g_c$, to g_0 well above the critical gain. In particular, for the experiments presented here, we have demonstrated tuning the cavity scale factor across a range, $1 < S_0 < 15$, with a corresponding tuning of the sensitivity across a range, $0.8 < \zeta_0 < 5.3$. The entire range of tuning was obtained in a single 3-cm ^{87}Rb vapor cell. Although one can also tune the cavity response by changing the finesse of the cavity, either through the reflectivity (r) of the cavity mirrors, or through a frequency-independent attenuation (a), tuning with the optical pumping method has the advantage of modifying the anomalous dispersion independently from the empty cavity mode width; hence, optical pumping allows for increasing the cavity sensitivity, even for a passive optical cavity.

[1] D. D. Smith, K. Myneni, J. A. Odutola, and J. C. Diels, Phys. Rev. A **80**, 011809R (2009).
[2] W. R. Bennett Jr., Phys. Rev. **126**, 580 (1962).
[3] R. A. McFarlane, Phys. Rev. **135**, A543 (1964).
[4] A. E. Siegman, *Lasers* (University Science Books, Sausalito, CA, 1986), pp. 466–471.
[5] M. D. Lukin, M. Fleischhauer, M. O. Scully, and V. L. Velichansky, Opt. Lett. **23**, 295 (1998).
[6] M. S. Shahriar, G. S. Pati, R. Tripathi, V. Gopal, M. Messall, and K. Salit, Phys. Rev. A **75**, 053807 (2007).
[7] D. D. Smith, H. Chang, L. Arissian, and J. C. Diels, Phys. Rev. A **78**, 053824 (2008).
[8] K. Myneni, D. D. Smith, J. A. Odutola, and C. A. Schambeau, *Proceedings of the 27th Army Science Conference, Orlando, FL* (Office of the Assistant Secretary of the Army, Acquisition, Logistics, and Technology, Washington, D.C., 2010).
[9] M. Salit, K. Salit, and P. Bauhahn, Opt. Exp. **19**, 25312 (2011).
[10] M. Salit, G. S. Pati, K. Salit, and M. S. Shahriar, J. Mod. Opt. **54**, 2425 (2007).
[11] G. S. Pati, M. Salit, K. Salit, and M. S. Shahriar, Opt. Commun. **281**, 4931 (2008).
[12] J. Gea-Banacloche, H. Wu, and M. Xiao, Phys. Rev. A **78**, 023828 (2008).
[13] Note that τ_0 can also be greater than unity for a gain medium, which we do not consider in this paper.
[14] F. W. King, J. Opt. Soc. Am. B **19**, 2427 (2002).
[15] Homogeneous broadening by collisions is entirely negligible for the low pressure, $\sim 10^{-7}$ Torr, found in the vapor cell at room temperature.
[16] P. Tremblay, J. Beaubien, A. Michaud, and E. Cauchon, J. Opt. Soc. Am. **9**, 1537 (1992).
[17] K. E. Gibble and A. Gallagher, Phys. Rev. A **43**, 1366 (1991).
[18] C. A. Schambeau, MS thesis, University of Alabama in Huntsville, 2009.
[19] K. Myneni, *Velocity-selective Optical Hyperfine Pumping in* ^{87}Rb (unpublished).
[20] These measurements were reported earlier in Ref. [8]; however, the method of fitting the data was subsequently found to be flawed. Fit parameters resulting from the correct fitting procedure are presented here.